Properties of a Single Photon Generated by a Solid-State Emitter: Effects of Pure Dephasing

Eiki Iyoda[1†], Takeo Kato[2], Takao Aoki[3], Keiichi Edamatsu[4], and Kazuki Koshino[1*]

[1]*College of Liberal Arts and Sciences, Tokyo Medical and Dental University, Ichikawa, Chiba 272-0827, Japan*
[2]*Institute for Solid State Physics, the University of Tokyo, Kashiwa, Chiba 277-8581, Japan*
[3]*Department of Applied Physics, Waseda University, Shinjuku, Tokyo 169-8555, Japan*
[4]*Research Institute of Electrical Communication, Tohoku University, Sendai 980-8577, Japan*

We investigate the properties of a single photon generated by a solid-state emitter subject to strong pure dephasing. We employ a model in which all the elements of the system, including the propagating fields, are treated quantum mechanically. We analytically derive the density matrix of the emitted photon, which contains full information about the photon, such as its pulse profile, power spectrum, and purity. We visualize these analytical results using realistic parameters and reveal the conditions for maximizing the purity of generated photons.

KEYWORDS: single-photon source, pure dephasing, purity

1. Introduction

Cavity quantum electrodynamics (QED) is currently one of the hottest research topics in atomic physics. In particular, quantum–mechanical interactions between atoms and cavity photons have been intensively studied.[1] Solid-state cavity QED systems composed of semiconductor quantum dots and cavities have recently been attracting much attention since they are suitable for creating compact optical devices.[2] Strong coupling between a single dot and a cavity has been confirmed through a large vacuum Rabi splitting.[3–5] This strong coupling has been applied to fabricate a single-dot laser[6] and to generate nonclassical light including single photons.[7–11] Excellent performances have been reported in generating indistinguishable photons[12,13] and entangled photon pairs,[14] both of which are useful for quantum information processing.[15]

In contrast to real atoms, semiconductor quantum dots are strongly influenced by environmental noise sources such as phonons and background carriers. The fluorescence spectra of solid-state and atomic cavity QED systems are qualitatively different. When a solid-state system is excited by pump light of the dot frequency, a spectral peak appears at the cavity frequency in spite of the large detuning between them.[3–5] This phenomenon has not been reported for atomic cavity QED systems. Further experimental studies have characterized this peak more thoroughly[16–22] and have revealed that the fluorescence at the cavity frequency is due to radiative decay of the dot. Subsequent theoretical studies accounted for the pure dephasing of the dot through the stochastic Schrödinger equation[23,24] or the Master equation[25–27] and successfully explained the peak at the cavity frequency. The influence of pure dephasing on the radiative decay of the dot can be understood in terms of the quantum Zeno and anti-Zeno effects.[25,28]

Therefore, when designing a single-photon source using solid-state cavity QED systems, it is crucial to quantitatively consider the pure dephasing of the dot. The performance of such photon sources should be evaluated from two aspects.

One is the collection efficiency, namely, the probability that the emitted photon is transferred to the intended spatial mode (i.e., the radiation pattern of the cavity). This has been discussed in several studies in terms of the ratio of radiative decay rates.[23,26,27] The other is the indistinguishability of generated photons, which can be measured by two-photon interference experiments and is evaluated by the purity. Single photons with high purity are required for quantum information processing, particularly for constructing scalable quantum circuits.

In this study, we investigate the properties of a single photon emitted by a solid-state cavity QED system and quantitatively observe the effects of pure dephasing. In order to obtain full information including the indistinguishability of generated single photons, we treat the five elements of the overall system (the dot, the cavity, radiation leaking from the cavity, non cavity radiation modes, and the environment causing the pure dephasing of the dot) as active quantum–mechanical degrees of freedom, and analytically derive the density matrix of the emitted photon in the real-space representation. This density matrix contains full information about the emitted photon, including its pulse profile, frequency spectrum, and purity. These quantities are observed as functions of the pure dephasing rate of the dot. We reveal the optimum condition for maximizing the purity of the emitted photon.

2. Model

We investigate the radiative decay of an excited quantum dot placed inside a cavity, as illustrated in Fig. 1. This solid-state cavity QED system consists of the following five components: (i) a quantum dot, (ii) a cavity, (iii) a photon field leaking from the cavity (referred to as b field hereafter), (iv) non-cavity radiation modes (c field), and (v) a reservoir field, which causes the pure dephasing of the dot (d field).[29] The annihilation operators corresponding to these components are respectively denoted as σ, a, b_k, c_k, and d_k, where k is a one-dimensional wave number. Note that σ is a Pauli operator, whereas the other operators are bosonic. Setting $\hbar = c = 1$, the Hamiltonian of the overall system is given by
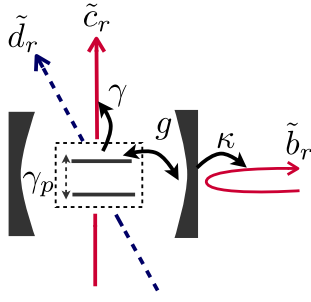
Fig. 1. (Color online) Schematic illustration of the solid-state cavity QED system considered. It consists of a quantum dot, a cavity, photon leakage from the cavity (*b* field), non-cavity radiation modes (*c* field), and a reservoir field, which causes the pure dephasing of the dot (*d* field).

$$\mathcal{H} = \mathcal{H}_0 + \mathcal{H}_1 + \mathcal{H}_2 + \mathcal{H}_3, \tag{1}$$

$$\mathcal{H}_0 = \omega_{\mathrm{d}}\sigma^\dagger\sigma + \omega_{\mathrm{c}}a^\dagger a + g(\sigma^\dagger a + a^\dagger\sigma), \tag{2}$$

$$\mathcal{H}_1 = \int \mathrm{d}k[k b_k^\dagger b_k + \sqrt{\kappa/(2\pi)}(a^\dagger b_k + b_k^\dagger a)], \tag{3}$$

$$\mathcal{H}_2 = \int \mathrm{d}k[k c_k^\dagger c_k + \sqrt{\gamma/(2\pi)}(\sigma^\dagger c_k + c_k^\dagger\sigma)], \tag{4}$$

$$\mathcal{H}_3 = \int \mathrm{d}k[k d_k^\dagger d_k + \sqrt{\gamma_{\mathrm{p}}/\pi}\sigma^\dagger\sigma(d_k^\dagger + d_k)]. \tag{5}$$

The parameters are defined as follows (see Fig. 1). ω_{d} and ω_{c} respectively denote the resonance frequencies of the dot and cavity, g represents the coupling between them, κ is the escape rate of cavity photons, γ is the radiative decay rate of the dot into non-cavity modes, and γ_{p} is the pure dephasing rate of the dot. $\mathcal{H}_0$ describes the Rabi oscillation between the dot and the cavity (Jaynes–Cummings Hamiltonian), $\mathcal{H}_1$ describes the leakage of a cavity photon to its radiation pattern, $\mathcal{H}_2$ describes the radiative decay of the dot in unintended directions, and $\mathcal{H}_3$ describes the pure dephasing of the dot. We can confirm that $\mathcal{N} \equiv \sigma^\dagger\sigma + a^\dagger a + \int \mathrm{d}r\, \widetilde{b}_r^\dagger \widetilde{b}_r + \int \mathrm{d}r\, \widetilde{c}_r^\dagger \widetilde{c}_r$ commutes with the Hamiltonian. Therefore, the number of excitations is conserved in the dot, cavity, and *b* and *c* fields.

We assume that the dot is initially ($t = 0$) in the excited state while the other fields are in their vacuum states. Then, denoting the overall vacuum state by $|0\rangle$, the initial state vector is given by

$$|\psi_i\rangle = \sigma^\dagger|0\rangle. \tag{6}$$

The Hamiltonian of Eq. (1) and the initial state vector of Eq. (6) form the basis of our analysis.

For later convenience, we introduce the real-space representation of the *b* field (cavity leakage). It is defined by

$$\widetilde{b}_r = (2\pi)^{-1/2}\int \mathrm{d}k\, \mathrm{e}^{\mathrm{i}kr} b_k. \tag{7}$$

The $r < 0$ ($r > 0$) region represents the incoming (outgoing) field. $\widetilde{c}_r$ and $\widetilde{d}_r$ can be formally defined in a similar manner. Our main concern lies in the properties of a single photon emitted in the *b* field.

To model the pure dephasing of the dot, the *d* field interacts with the dot so as to conserve the dot excitation. Using Eqs. (2) and (5), the dot Hamiltonian can be rewritten as $[\omega_{\mathrm{d}} + f(t)]\sigma^\dagger\sigma$, where $f(t) = \sqrt{2\gamma_{\mathrm{p}}}[\widetilde{d}_0(t) + \widetilde{d}_0^\dagger(t)]$ is the fluctuation of the dot resonance frequency induced by the

d field. Using Eqs. (6) and (10), we can confirm that $\langle f(t)f(t')\rangle_i = 2\gamma_{\mathrm{p}}\delta(t - t')$, where $\langle \cdots \rangle_i = \langle \psi_i | \cdots | \psi_i \rangle$. Therefore, the present model assumes a white noise spectrum for the fluctuation of the dot resonance.

3. Analysis

In this section, we present analytical results that are rigorously derivable from the model described in Sect. 2. We solve the time evolution of the overall system within the input–output formalism[30,31] and derive several formulae to characterize the emitted single photon (density matrix, pulse shape, spectrum, and purity). These analytical results are visualized in the next section for specific parameters.

3.1 Heisenberg equations

Here, we present the Heisenberg equations for the system (σ, a) and field (b_k, c_k, d_k) operators. Deriving the raw Heisenberg equations for the field operators from Eq. (1) and transforming them into real-space representations, we obtain the following relations that connect the incoming ($r < 0$) and outgoing ($r > 0$) fields:

$$\widetilde{b}_r(t) = \widetilde{b}_{r-t}(0) - \mathrm{i}\sqrt{\kappa}\theta(r)\theta(t - r)a(t - r), \tag{8}$$

$$\widetilde{c}_r(t) = \widetilde{c}_{r-t}(0) - \mathrm{i}\sqrt{\gamma}\theta(r)\theta(t - r)\sigma(t - r), \tag{9}$$

$$\widetilde{d}_r(t) = \widetilde{d}_{r-t}(0) - \mathrm{i}\sqrt{2\gamma_{\mathrm{p}}}\theta(r)\theta(t - r)\sigma^\dagger(t - r)\sigma(t - r), \tag{10}$$

where $\theta(x)$ is the Heaviside step function. From the raw Heisenberg equations for the system operators and the above input–output relations, the Heisenberg equations for system operators are given by

$$\frac{\mathrm{d}}{\mathrm{d}t}\sigma = -\mathrm{i}\widetilde{\omega}_{\mathrm{d}}\sigma - \mathrm{i}g(1 - 2\sigma^\dagger\sigma)a - \mathrm{i}(1 - 2\sigma^\dagger\sigma)N_{\mathrm{c}}(t) \\ - \mathrm{i}[N_{\mathrm{d}}^\dagger(t)\sigma + \sigma^\dagger N_{\mathrm{d}}(t)], \tag{11}$$

$$\frac{\mathrm{d}}{\mathrm{d}t}a = -\mathrm{i}\widetilde{\omega}_{\mathrm{c}}a - \mathrm{i}g\sigma - \mathrm{i}N_{\mathrm{b}}(t), \tag{12}$$

where $\widetilde{\omega}_{\mathrm{d}} = \omega_{\mathrm{d}} - \mathrm{i}(\gamma/2 + \gamma_{\mathrm{p}})$ and $\widetilde{\omega}_{\mathrm{c}} = \omega_{\mathrm{c}} - \mathrm{i}\kappa/2$ respectively are the complex frequencies of the dot and cavity, and the noise operators are defined by $N_{\mathrm{b}}(t) = \sqrt{\kappa}\widetilde{b}_{-t}(0)$, $N_{\mathrm{c}}(t) = \sqrt{\gamma}\widetilde{c}_{-t}(0)$, and $N_{\mathrm{d}}(t) = \sqrt{2\gamma_{\mathrm{p}}}\widetilde{d}_{-t}(0)$. Note that the noise operators are the initial-time operators and, consequently, $N_j(t)|0\rangle = 0$ ($j = b, c, d$).

3.2 State vector

The state vector of the overall system at an arbitrary time t is determined by $|\psi(t)\rangle = \mathrm{e}^{-\mathrm{i}\mathcal{H}t}|\psi(0)\rangle$. Since the initial dot excitation is conserved in the dot, cavity, and *b* and *c* fields, the state vector can be written as

$$|\psi(t)\rangle = \left[\alpha_0(t)\sigma^\dagger + \beta_0(t)a^\dagger + \int \mathrm{d}r\, \gamma_0(r, t)\widetilde{b}_r^\dagger \right. \\ \left. + \int \mathrm{d}r\, \delta_0(r, t)\widetilde{c}_r^\dagger \right]|0\rangle \\ + \sum_{m=1}^{\infty}\int \mathrm{d}^m\boldsymbol{x}\left[\alpha_m(\boldsymbol{x}, t)\sigma^\dagger + \beta_m(\boldsymbol{x}, t)a^\dagger \right. \\ + \int \mathrm{d}r\, \gamma_m(r, \boldsymbol{x}, t)\widetilde{b}_r^\dagger \\ \left. + \int \mathrm{d}r\, \delta_m(r, \boldsymbol{x}, t)\widetilde{c}_r^\dagger \right]\widetilde{d}_{x_1}^\dagger \cdots \widetilde{d}_{x_m}^\dagger|0\rangle, \tag{13}$$

where m denotes the number of excitations in the *d* field and $\int \mathrm{d}^m\boldsymbol{x}$ denotes a multi-dimensional integral with respect to

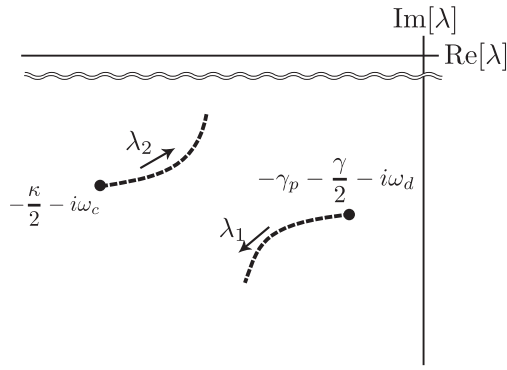Fig. 2. λ_1 and λ_2 in the complex plane. $\lambda_1 = -i\widetilde{\omega}_d$ and $\lambda_2 = -i\widetilde{\omega}_c$ when $g = 0$. Dotted lines show their traces as g increases.

Fig. 3. μ_j ($j = 1, \ldots, 4$) in the complex plane. When γ_p is absent, $\mu_1 = \lambda_1 + \lambda_1^*$, $\mu_2 = \lambda_1 + \lambda_2^*$, $\mu_3 = \lambda_2 + \lambda_1^*$, and $\mu_4 = \lambda_2 + \lambda_2^*$. Dotted lines indicate their traces as γ_p increases. Real parts of μ_j are always negative for any γ_p.

$\boldsymbol{x} = (x_1, x_2, \ldots, x_m)$. We can set $x_1 \leq \cdots \leq x_m$ without loss of generality. As we show later, these coefficients are nonzero only when $0 \leq r \leq x_1 \leq \cdots \leq x_m \leq t$.

First, we discuss α_0 and β_0. From Eq. (13), we can confirm that $\alpha_0(t) = \langle \sigma(t)\sigma^\dagger(0) \rangle$ and $\beta_0(t) = \langle c(t)\sigma^\dagger(0) \rangle$, where $\langle \cdots \rangle = \langle 0 | \cdots | 0 \rangle$. From Eqs. (11) and (12), their equations of motion are given by

$$\frac{d}{dt}\begin{pmatrix} \alpha_0(t) \\ \beta_0(t) \end{pmatrix} = \begin{pmatrix} -i\widetilde{\omega}_d & -ig \\ -ig & -i\widetilde{\omega}_c \end{pmatrix}\begin{pmatrix} \alpha_0(t) \\ \beta_0(t) \end{pmatrix}, \quad (14)$$

with the initial conditions $\alpha_0(0) = 1$ and $\beta_0(0) = 0$. The solutions are given by

$$\alpha_0(t) = A_1 e^{\lambda_1 t} + A_2 e^{\lambda_2 t}, \quad (15)$$

$$\beta_0(t) = B_1 e^{\lambda_1 t} + B_2 e^{\lambda_2 t}, \quad (16)$$

where λ_1 and λ_2 are the two eigenvalues of the 2×2 matrix in Eq. (14) (see Fig. 2), $A_1 = (\lambda_1 + i\widetilde{\omega}_c)/(\lambda_1 - \lambda_2)$, $A_2 = (\lambda_2 + i\widetilde{\omega}_c)/(\lambda_2 - \lambda_1)$, and $B_1 = -B_2 = -ig/(\lambda_1 - \lambda_2)$. The real parts of λ_1 and λ_2 are always negative and, consequently, α_0 and β_0 vanish as $t \to \infty$. Equation (13) also implies that $\gamma_0(r, t) = \langle \widetilde{b}_r(t)\sigma^\dagger(0) \rangle$ and $\delta_0(r, t) = \langle \widetilde{c}_r(t)\sigma^\dagger(0) \rangle$. From Eqs. (8) and (9), we have

$$\gamma_0(r, t) = -i\sqrt{\kappa}\beta_0(t - r), \quad (17)$$

$$\delta_0(r, t) = -i\sqrt{\gamma}\alpha_0(t - r). \quad (18)$$

Rigorously, $\theta(r)\theta(t - r)$ should appear on the right-hand sides of these equations. However, below, we implicitly assume $0 \leq r \leq x_1 \leq \cdots \leq x_m \leq t$ and omit the Heaviside functions.

Next, we proceed to investigate higher-order quantities including reservoir (d field) excitations. We consider α_1 and β_1 as examples. Applying the same reasoning as that for γ_0 and δ_0, we have $\alpha_1(x, t) = -i\sqrt{2\gamma_p}\langle \sigma(t)\sigma^\dagger(t - x)\sigma(t - x)\sigma^\dagger(0) \rangle$ and $\beta_1(x, t) = -i\sqrt{2\gamma_p}\langle a(t)\sigma^\dagger(t - x)\sigma(t - x)\sigma^\dagger(0) \rangle$. Thus, we must evaluate the three-time correlation functions $\langle \sigma(t_2)\sigma^\dagger(t_1)\sigma(t_1)\sigma^\dagger(0) \rangle$ and $\langle a(t_2)\sigma^\dagger(t_1)\sigma(t_1)\sigma^\dagger(0) \rangle$ with $t_2 > t_1 > 0$. Their equations of motion with respect to t_2 have the same form as Eq. (14) and their initial values ($t_2 \to t_1$) are $\alpha_0(t_1)$ and 0, respectively. This implies that the two-time correlation functions can be factorized as $\langle \sigma(t_2)\sigma^\dagger(t_1)\sigma(t_1)\sigma^\dagger(0) \rangle = \alpha_0(t_2 - t_1)\alpha_0(t_1)$ and $\langle a(t_2)\sigma^\dagger(t_1)\sigma(t_1)\sigma^\dagger(0) \rangle = \beta_0(t_2 - t_1)\alpha_0(t_1)$. Thus, we have

$$\alpha_1(x, t) = -i\sqrt{2\gamma_p}\alpha_0(t - x)\alpha_0(x), \quad (19)$$

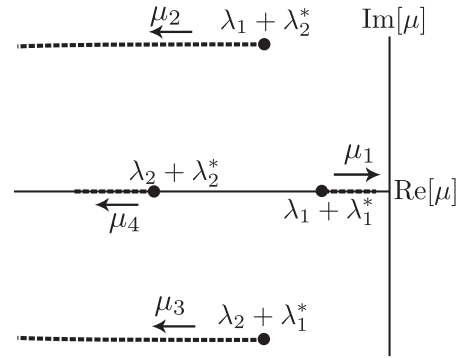$$\beta_1(x, t) = -i\sqrt{2\gamma_p}\alpha_0(t - x)\beta_0(x). \quad (20)$$

Repeating the same arguments, all coefficients can be written as products of α_0 and β_0, as follows:

$$\alpha_m(\boldsymbol{x}, t) = (-i\sqrt{2\gamma_p})^m K_m(\boldsymbol{x}, t)\alpha_0(x_1), \quad (21)$$

$$\beta_m(\boldsymbol{x}, t) = (-i\sqrt{2\gamma_p})^m K_m(\boldsymbol{x}, t)\beta_0(x_1), \quad (22)$$

$$\gamma_m(r, \boldsymbol{x}, t) = (-i\sqrt{\kappa})(-i\sqrt{2\gamma_p})^m K_m(\boldsymbol{x}, t)\beta_0(x_1 - r), \quad (23)$$

$$\delta_m(r, \boldsymbol{x}, t) = (-i\sqrt{\gamma})(-i\sqrt{2\gamma_p})^m K_m(\boldsymbol{x}, t)\alpha_0(x_1 - r), \quad (24)$$

where

$$K_m(\boldsymbol{x}, t) = \alpha_0(t - x_m)\alpha_0(x_m - x_{m-1}) \cdots \alpha_0(x_2 - x_1). \quad (25)$$

3.3 Decay of dot excitation

The state vector of Eq. (13) fully describes the dynamics of the overall system, including both its transient and asymptotic behaviors. In this section, as an example of a transient phenomenon, we analyze the decay of dot excitation. The survival probability of dot excitation is defined as $P(t) = \langle \psi(t) | \sigma^\dagger \sigma | \psi(t) \rangle$. From Eqs. (13) and (21), we have

$$P(t) = |\alpha_0(t)|^2 + 2\gamma_p \int dx |\alpha_0(t - x)|^2 |\alpha_0(x)|^2 + \cdots. \quad (26)$$

We here introduce the Laplace transform of $|\alpha_0|^2$, which is defined by $\mathcal{L}_{|\alpha_0|^2}(z) = \int_0^\infty dt\, e^{-zt}|\alpha_0(t)|^2$. It is given by

$$\mathcal{L}_{|\alpha_0|^2}(z) = \sum_{m,n=1,2} \frac{A_m A_n^*}{z - \lambda_m - \lambda_n^*}, \quad (27)$$

where $\lambda_{1,2}$ and $A_{1,2}$ are defined in Sect. 3.2. The Laplace transform of $P(t)$ is then given by

$$\mathcal{L}_P(z) = \frac{\mathcal{L}_{|\alpha_0|^2}(z)}{1 - 2\gamma_p \mathcal{L}_{|\alpha_0|^2}(z)}. \quad (28)$$

$P(t)$ is obtained by analyzing the poles of this function in the z-plane. We denote the four roots of the equation $1 - 2\gamma_p \mathcal{L}_{|\alpha_0|^2}(z) = 0$ by μ_j ($j = 1, \ldots, 4$) (see Fig. 3). $P(t)$ is then given by

$$P(t) = \sum_{j=1}^4 E_j e^{\mu_j t}, \quad (29)$$

$$E_j = \frac{\prod_{m',n'=1,2}(\mu_j - \lambda_{m'} - \lambda_{n'}^*)}{\prod_{i(\neq j)}(\mu_j - \mu_i)} \sum_{m,n=1,2} \frac{A_m A_n^*}{\mu_j - \lambda_m - \lambda_n^*}. \quad (30)$$

Note that the real parts of μ_j are always negative and that the survival probability $P(t)$ vanishes in the $t \to \infty$ limit, as expected.

3.4 Density matrix of emitted photon

In the $t \to \infty$ limit, the initial dot excitation is completely transformed into a photon propagating in the intended mode (b field) or in unintended directions (c field). In the following subsections, we analyze the photon emitted in the b field. It is fully characterized by its density matrix $\hat{\rho}(t)$. In the real-space representation, the matrix element $\rho(r, r', t)$ is given by

$$\rho(r, r', t) = \langle \psi(t) | \widetilde{b}_{r'}^{\dagger} \widetilde{b}_r | \psi(t) \rangle. \tag{31}$$

We make the following three comments regarding this quantity: (i) $\hat{\rho}(t)$ is Hermitian, namely, $\rho(r', r, t) = \rho^*(r, r', t)$. Therefore, we need consider only the $r < r'$ region in this subsection. (ii) As we will see later, $\rho(r, r', t) = \rho(r - t, r' - t)$ in the $t \to \infty$ limit. This reflects the translational motion of the emitted photon. (iii) $\mathrm{Tr}\,\hat{\rho}(t) = \int \mathrm{d}r\, \rho(r, r, t)$ represents the probability of finding the emitted photon in the b field. This is unity when $\gamma = 0$.

Using Eqs. (13) and (23), the matrix element can be rewritten as

$$\begin{aligned}
\rho(r, r', t) = &\, \kappa \beta_0(t - r)\beta_0^*(t - r') \\
&+ 2\gamma_{\mathrm{p}}\kappa \int \mathrm{d}x\, \beta_0(x - r)\beta_0^*(x - r')|\alpha_0(t - x)|^2 \\
&+ \cdots.
\end{aligned} \tag{32}$$

We here introduce the Laplace transform of $\beta_0 \beta_0^*$, which is defined by $\mathcal{L}_{\beta_0 \beta_0^*}(r, r', z) = \int_0^\infty \mathrm{d}t\, e^{-zt}\beta_0(t - r)\beta_0^*(t - r')$. It is given by

$$\mathcal{L}_{\beta_0 \beta_0^*}(r, r', z) = \sum_{m,n=1,2} \frac{B_m B_n^*}{z - \lambda_m - \lambda_n^*} e^{\lambda_m(r' - r) - r'z}, \tag{33}$$

where $\lambda_{1,2}$ and $B_{1,2}$ are defined in Sect. 3.2. The Laplace transform of $\rho(r, r', t)$ is then given by

$$\mathcal{L}_\rho(r, r', z) = \frac{\kappa \mathcal{L}_{\beta_0 \beta_0^*}(r, r', z)}{1 - 2\gamma_{\mathrm{p}}\mathcal{L}_{|\alpha_0|^2}(z)}. \tag{34}$$

By analyzing the poles of this function in the z-plane, $\rho(r, r', t)$ is obtained as follows:

$$\rho(r, r', t) = \sum_{j=1}^{4} \sum_{m=1}^{2} \rho_{jm} e^{\lambda_m(r' - r) + \mu_j(t - r')}, \tag{35}$$

$$\rho_{jm} = \frac{\displaystyle\prod_{m',n'=1,2}(\mu_j - \lambda_{m'} - \lambda_{n'}^*)}{\displaystyle\prod_{i(\neq j)}(\mu_j - \mu_i)} \sum_{n=1}^{2} \frac{B_m B_n^*}{\mu_j - \lambda_m - \lambda_n^*}, \tag{36}$$

where $0 < r < r' < t$ and μ_j $(j = 1, \ldots, 4)$ are defined in Sect. 3.3. We can check that this quantity depends on only two variables, $r - t$ and $r' - t$.

3.5 Pulse shape

The pulse shape of the emitted photon is characterized by the intensity distribution $f(r, t) = \langle \psi(t) | \widetilde{b}_r^{\dagger} \widetilde{b}_r | \psi(t) \rangle = \rho(r, r, t)$, which is the diagonal element of the density matrix. This quantity is real and positive for $0 < r < t$. By setting $r' = r$ in Eq. (35), we have

$$f(r, t) = \sum_{j=1}^{4} f_j e^{\mu_j(t - r)}, \tag{37}$$

$$f_j = \frac{\displaystyle\prod_{m',n'=1,2}(\mu_j - \lambda_{m'} - \lambda_{n'}^*)}{\displaystyle\prod_{i \neq j}(\mu_j - \mu_i)} \sum_{m,n=1}^{2} \frac{B_m B_n^*}{\mu_j - \lambda_m - \lambda_n^*}. \tag{38}$$

3.6 Frequency spectrum

The frequency spectrum of the emitted photon is defined by $S(k, t) = \langle \psi(t) | b_k^{\dagger} b_k | \psi(t) \rangle$. Apparently, $S(k, t)$ becomes independent of t in the $t \to \infty$ limit, and we are interested in $S(k) = \lim_{t \to \infty} S(k, t)$. By definition, $S(k, t)$ is the Fourier transform of the density matrix element:

$$S(k, t) = \frac{1}{2\pi} \iint \mathrm{d}r\,\mathrm{d}r'\, e^{ik(r' - r)}\rho(r, r', t). \tag{39}$$

We consider the Laplace transform of $S(k, t)$ defined by $\mathcal{L}_S(k, z) = \int_0^\infty \mathrm{d}t\, e^{-zt}S(k, t)$. Using Eqs. (34) and (39), it is given by

$$\mathcal{L}_S(k, z) = \frac{\kappa}{2\pi} \frac{\mathcal{L}'_{\beta_0 \beta_0^*}(k, z)}{1 - 2\gamma_{\mathrm{p}}\mathcal{L}_{|\alpha_0|^2}(z)}, \tag{40}$$

where

$$\begin{aligned}
\mathcal{L}'_{\beta_0 \beta_0^*}(k, z) &= \int_0^\infty \mathrm{d}t \iint \mathrm{d}r\,\mathrm{d}r'\, e^{ik(r' - r) - zt}\beta_0^*(t - r')\beta_0^*(t - r) \\
&= \int_0^\infty \mathrm{d}t\, e^{-zt} \left| \sum_{m=1}^{2} \frac{B_m}{\lambda_m + ik}(e^{-ikt} - e^{\lambda_m t}) \right|^2.
\end{aligned} \tag{41}$$

Note that $\mathcal{L}'_{\beta_0 \beta_0^*}$ has a pole at $z = 0$. Since our interest lies in the $t \to \infty$ limit of $S(k, t)$, we must investigate the pole of $\mathcal{L}_S(k, z)$ at $z = 0$ only. Therefore, $S(k) = (\kappa/2\pi)[1 - 2\gamma_{\mathrm{p}}\mathcal{L}_{|\alpha_0|^2}(0)]^{-1}\,\mathrm{Res}_{z=0}[\mathcal{L}'_{\beta_0 \beta_0^*}(k, z)]$. After some calculations, we obtain

$$S(k) = \frac{\mathcal{N}}{|(k - \widetilde{\omega}_{\mathrm{d}})(k - \widetilde{\omega}_{\mathrm{c}}) - g^2|^2}, \tag{42}$$

where $\mathcal{N} = (\kappa g^2/2\pi)[1 - 2\gamma_{\mathrm{p}}\mathcal{L}_{|\alpha_0|^2}(0)]^{-1}$ is a factor that is independent of k. This spectral shape was predicted by Glauber,[32] and it was confirmed in recent theoretical studies based on the quantum Langevin equations[23,24] and the Master equations.[25–27] The relation to the Master equation approach is summarized in Appendix A.

3.7 Purity

Quantum information processing requires high indistinguishability between single photons. A popular measure of the indistinguishability of photons is the coincidence probability P_{co} in two-photon interference experiments (see Fig. 4). Two solid-state emitters simultaneously emit single photons into two input ports of a beam splitter. These two photons are mixed by the beam splitter and are counted by photo detectors. When two indistinguishable photons are simultaneously input to a beam splitter, they always appear at the same output port (Hong–Ou–Mandel interference), namely, $P_{\mathrm{co}} = 0$. However, pure dephasing generates entanglement between an emitted photon and the environment of its source, making two-photon interference imperfect ($P_{\mathrm{co}} > 0$). The coincidence probability is related to the purity $\mathcal{P}$ of a photon by $P_{\mathrm{co}} = (1 - \mathcal{P})/2$ (see Appendix C for the derivation).

The purity is defined in terms of the density matrix $\hat{\rho}(t)$ by $\mathcal{P} = \mathrm{Tr}[\hat{\rho}^2(t)]$. As expected, this quantity becomes indepen-
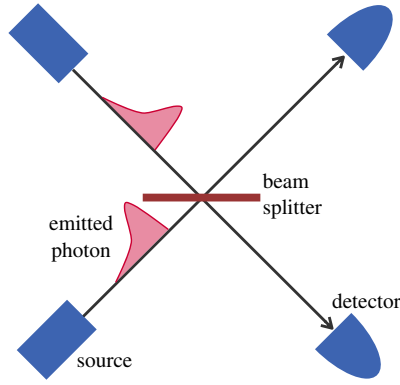
Fig. 4. (Color online) Schematic illustration of two-photon interference experiment. The coincidence probability vanishes when the two input photons are completely indistinguishable.
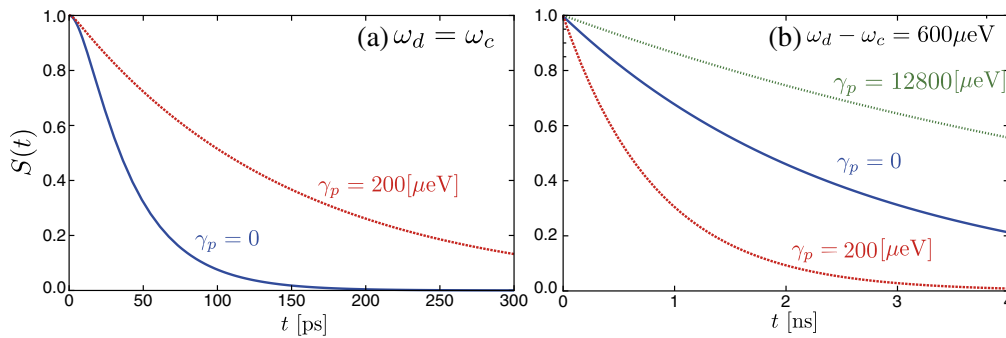

Fig. 6. (Color online) Dependence of the radiative decay rate $\bar{\Gamma}$ on the pure dephasing rate γ_{p}. The radiative decay rate is normalized by the *free* decay rate (i.e., the rate for $\gamma_{\mathrm{p}} = 0$). $g = 25\,\mu\mathrm{eV}$ and $\kappa = 150\,\mu\mathrm{eV}$. $\omega_{\mathrm{d}} - \omega_{\mathrm{c}} = 0$ (solid), 66 (dotted), and $150\,\mu\mathrm{eV}$ (dashed).

Fig. 5. (Color online) Survival probability $S(t)$ for (a) resonant ($\omega_{\mathrm{d}} = \omega_{\mathrm{c}}$) and (b) detuned ($\omega_{\mathrm{d}} - \omega_{\mathrm{c}} = 600\,\mu\mathrm{eV}$) cases. $g = 25\,\mu\mathrm{eV}$ and $\kappa = 150\,\mu\mathrm{eV}$. The values of γ_{p} are indicated in the figures.

dent of t when t is sufficiently large. Using the real-space matrix element, the purity can be rewritten as

$$\mathcal{P} = \lim_{t \to \infty} \int \mathrm{d}r\, \mathrm{d}r'\, \rho(r, r', t) \rho(r', r, t)$$

$$= \lim_{t \to \infty} \int \mathrm{d}r\, \mathrm{d}r' |\rho(r, r', t)|^2. \qquad (43)$$

Using Eq. (36), we have

$$\mathcal{P} = \sum_{j, j'=1}^{4} \sum_{m, m'=1}^{2} \frac{2\rho_{jm}\rho_{j'm'}^*}{(\mu_j + \mu_{j'}^*)(\lambda_m + \lambda_{m'}^*)}. \qquad (44)$$

4. Numerical Results

The analytical results derived in the previous section are rigorous and applicable to any set of parameters, $(\omega_{\mathrm{d}} - \omega_{\mathrm{c}}, g, \kappa, \gamma, \gamma_{\mathrm{p}})$. In this section, we visualize these results by employing specific parameters. Throughout this section, we assume, for simplicity, that radiative decay to unintended modes does not occur ($\gamma = 0$).

4.1 Zeno and anti-Zeno effects

First, we observe the effects of pure dephasing on the decay of dot excitation. We focus on the weak-coupling regime ($\kappa = 6g$) in this subsection, where the dot decays monotonically without revival and obeys the exponential decay law with high accuracy. The decay rate of the dot is well defined in this case and is given by $\Gamma = \lim_{t \to \infty}[-\log P(t)/t]$. This reduces to $\min_j |\operatorname{Re} \mu_j|$, where
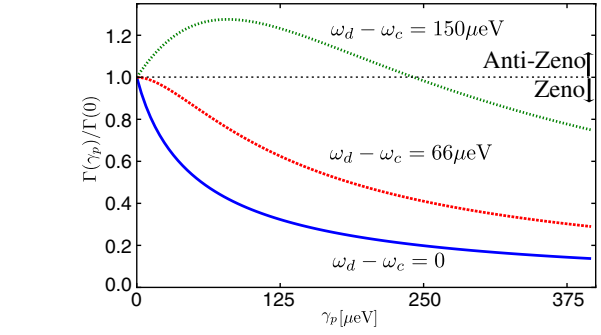
μ_j is defined in Sect. 3.3. Figure 5 shows the temporal behavior of the survival probability $P(t)$. In Fig. 5(a), where the dot is in resonance with the cavity ($\omega_{\mathrm{d}} = \omega_{\mathrm{c}}$), the decay becomes slower as pure dephasing increases. In contrast, in Fig. 5(b), where the dot is detuned from the cavity ($\omega_{\mathrm{d}} - \omega_{\mathrm{c}} = 600\,\mu\mathrm{eV}$), the decay becomes faster under small pure dephasing ($\gamma_{\mathrm{p}} = 200\,\mu\mathrm{eV}$), whereas the decay becomes slower under larger pure dephasing ($\gamma_{\mathrm{p}} = 12800\,\mu\mathrm{eV}$).

Measurements to check the survival of dot excitation destroy the quantum coherence between the excited and ground states that preserves the population of these two states. Therefore, pure dephasing has the same effect on the dot as continuous measurements, if the measurement results are unquestioned. The changes in the decay rates induced by pure dephasing are often interpreted as the quantum Zeno and anti-Zeno effects.[25,33,34] Previous analyses indicated that the anti-Zeno effect can be observed only when the dot–cavity detuning is large and pure dephasing is small.[28] This agrees with the present numerical results. Figure 6 shows the dependence of the radiative decay rate Γ on the pure dephasing rate γ_{p}. To clearly observe the Zeno and anti-Zeno effects, $\Gamma(\gamma_{\mathrm{p}})$ is normalized by the *free* decay rate of $\Gamma(0)$; $\Gamma(\gamma_{\mathrm{p}})/\Gamma(0) < 1$ indicates the Zeno effect, whereas $\Gamma(\gamma_{\mathrm{p}})/\Gamma(0) > 1$ exhibits the anti-Zeno effect. Non monotonic behavior of $\Gamma(\gamma_{\mathrm{p}})$ is clearly observed for large detuning.

4.2 Pulse shape and spectrum

In this subsection, we examine the pulse shape and

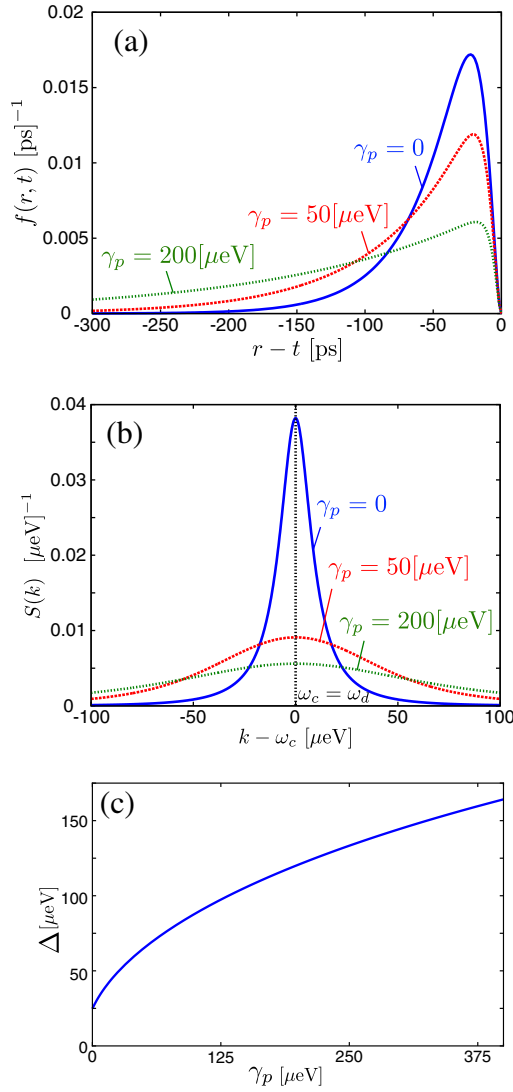   ©2013 The Physical Society of Japan

Fig. 7. (Color online) (a) Pulse shape $f(r,t)$ and (b) spectrum $S(k)$ of emitted photon. $g = 25\,\mu\text{eV}$, $\kappa = 150\,\mu\text{eV}$, and $\omega_\text{d} - \omega_\text{c} = 0$. $\gamma_\text{p} = 0$ (solid), 50 (dotted), and 200 μeV (dashed). (c) Spectral width as a function of γ_p.
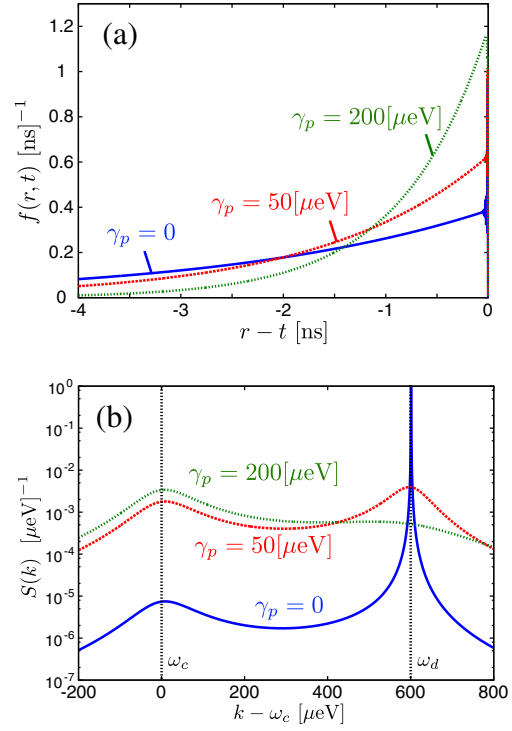

Fig. 8. (Color online) (a) Pulse shape $f(r,t)$ and (b) spectrum $S(k)$ of emitted photon. $g = 25\,\mu\text{eV}$, $\kappa = 150\,\mu\text{eV}$, and $\omega_\text{d} - \omega_\text{c} = 600\,\mu\text{eV}$. $\gamma_\text{p} = 0$ (solid), 50 (dotted), and 200 μeV (dashed).

frequency spectrum of the emitted photon using the same parameters as those used in the previous subsection. First, we observe the results for the resonant ($\omega_\text{d} = \omega_\text{c}$) case. The pulse shapes $f(r,t)$ of the emitted photon are shown in Fig. 7(a) for three pure dephasing rates γ_p. Each pulse shape is normalized $[\int_{-\infty}^{t} dr\, f(r,t) = 1]$ since $\gamma = 0$ is assumed here and a single photon is necessarily generated in the b field. The pulse becomes longer as pure dephasing increases. This is consistent with the quantum Zeno effect discussed in the previous subsection: in the resonant case, the decay of the dot becomes monotonically slower with increasing pure dephasing. Figure 7(b) shows the spectra $S(k)$ of the photon for the same parameters as those in Fig. 7(a). These spectra have a single peak at $k = \omega_\text{d}$ ($= \omega_\text{c}$) and are normalized $[\int_{-\infty}^{\infty} dk\, S(k) = 1]$. The spectrum broadens with increasing pure dephasing. This is confirmed by Fig. 7(c), in which the spectral width (defined as $\Delta = [\int dk(k - \omega_\text{d})^2 S(k)]^{1/2}$) is plotted as a function of the pure dephasing rate. Thus, the pulse broadens in both the real and frequency spaces with increasing γ_p and it is thus not Fourier-limited. This implies

that the emitted photon is in a mixed state when $\gamma_\text{p} \neq 0$. The purity of the photon is discussed later in Sect. 4.3.

Next, we observe the results for the detuned case. Figure 8(a) shows the pulse shapes of the photon. The pulse shape is approximately exponential, except for the oscillatory behavior at the very initial stage. The pulse length is inversely proportional to the decay rate of the dot. Figure 8(b) shows the photon spectra for the same parameters as those in Fig. 8(a). A notable difference from the resonant case is that the spectra are doubly peaked with peaks at both the dot frequency ω_d and the cavity frequency ω_c. The widths of these peaks are determined by $|\,\text{Im}\,\widetilde{\omega}_\text{d}\,| = \gamma/2 + \gamma_\text{p}$ and $|\,\text{Im}\,\widetilde{\omega}_\text{c}\,| = \kappa/2$. Therefore, the width of the peak at ω_d is sensitive to pure dephasing. When pure dephasing is weak ($\gamma_\text{p} \ll \kappa$), as in atomic cavity QED systems, the dominant peak of $S(k)$ appears at ω_d. In contrast, when pure dephasing is strong ($\gamma_\text{p} \gg \kappa$), as in solid-state systems, the dominant peak of $S(k)$ appears at ω_c. This behavior can be seen more clearly in an approximate form of the spectrum,

$$S(k) = \frac{2\gamma_\text{p}}{2\gamma_\text{p} + \kappa} S_\text{cav}(k) + \frac{\kappa}{2\gamma_\text{p} + \kappa} S_\text{dot}(k), \quad (45)$$

$$S_\text{cav}(k) = \frac{\kappa/2\pi}{(k - \omega_\text{c})^2 + (\kappa/2)^2}, \quad (46)$$

$$S_\text{dot}(k) = \frac{\gamma_\text{p}/\pi}{(k - \omega_\text{d})^2 + \gamma_\text{p}^2}, \quad (47)$$

which is valid for $|\omega_\text{d} - \omega_\text{c}| \gg g$. From this expression, it is proved that the cavity spectrum S_cav is dominant for $\gamma_\text{p} \gg \kappa$, whereas the dot spectrum S_dot is dominant for $\gamma_\text{p} \ll \kappa$. This result partly explains the detuned peaks observed in the resonance fluorescence spectrum in solid-state cavity QED systems, as discussed in previous theoretical works.[23–25]

The mean energy of the emitted photon is evaluated by $E_{\rm p} = \int {\rm d}k\, k\, S(k)$. Owing to energy conservation, the mean photon energy is expected to always be identical to the dot frequency (i.e., $E_{\rm p} = \omega_{\rm d}$). However, Fig. 8(b) clearly shows that the mean photon energy is sensitive to pure dephasing and may deviate from the dot frequency when pure dephasing is present. This discrepancy can be resolved by considering the energy released to the environment during decay, which is given by $E_{\rm e} = \int {\rm d}k\, k\, \langle d_k^\dagger d_k \rangle$. It can be shown that (see Appendix D for derivation)

$$E_{\rm p} = \frac{2\gamma_{\rm p}}{\kappa + 2\gamma_{\rm p}}\omega_{\rm c} + \frac{\kappa}{\kappa + 2\gamma_{\rm p}}\omega_{\rm d}, \quad (48)$$

$$E_{\rm e} = \frac{2\gamma_{\rm p}}{\kappa + 2\gamma_{\rm p}}(\omega_{\rm d} - \omega_{\rm c}). \quad (49)$$

Thus, energy conservation is satisfied when the environmental energy is included ($E_{\rm p} + E_{\rm e} = \omega_{\rm d}$). It should be noted that while pure dephasing coupling never induces a transition in the dot, this coupling enables energy exchange between the dot and the environment. When the cavity frequency exceeds the dot frequency, Eq. (49) indicates that the dot may absorb environmental energy during decay.[29]

4.3 Purity

As discussed in Sect. 3.7, the coincidence probability in two-photon interference $P_{\rm co}$, which is a popular measure of indistinguishability, is related to the purity as $P_{\rm co} = (1 - \mathcal{P})/2$. In this subsection, we show numerical results for the purity $\mathcal{P}$ for various parameter regions. Qualitative features in some limiting cases are discussed in Appendix B on the basis of perturbation calculation.

We first consider the resonant case ($\omega_{\rm c} = \omega_{\rm d}$). In Fig. 9(a), the purity $\mathcal{P}$ is plotted as a function of κ and $\gamma_{\rm p}$. The purity becomes large for $\gamma_{\rm p} < \min(\kappa/2, 2g^2/\kappa)$ (the region below "Line 1" in the figure). From the figure, we can see that for the generation of coherent photons, pure dephasing should be reduced as much as possible, and that for fixed pure dephasing, κ should be taken near the point of critical damping ($\kappa = 2g$). In addition to this main region appropriate for highly coherent photon generation, there is a line on which the purity has a small peak (denoted as "Line 2" in the figure) in the region of $\gamma_{\rm p} \gg g$. By perturbation calculation (see Appendix B), we can show that the purity takes a maximum value of $\mathcal{P}_{\rm max} = 3 - 2\sqrt{2} \simeq 0.17$ at $\gamma_{\rm p} = 2\sqrt{2}g^2/\kappa$.

Next, we consider the strongly detuned case ($|\omega_{\rm d} - \omega_{\rm c}| \gg g$). In Fig. 9(b), the purity is shown as a function of κ and $\gamma_{\rm p}$ for $\omega_{\rm d} - \omega_{\rm c} = 8g$. The purity has a large value below the line $\gamma_{\rm p} < \min(\varepsilon\kappa/2, 2g^2/\kappa)$ (the region below "Line 1" in the figure), where $\varepsilon = g^2/(\omega_{\rm d} - \omega_{\rm c})^2$ is a small parameter dependent on detuning. In Fig. 9(b), we can see that the purity for the detuned case is suppressed compared with the resonant case, and that the high-purity region is narrowed. From the figure, we can see that for coherent photon emission, dephasing should be reduced as much as possible, and that for fixed pure dephasing, κ should be taken to be around $\kappa = (2\sqrt{2}g^2/\varepsilon)^{1/2}$. In addition to the main high-purity region, the purity has a small peak (denoted as "Line 2") similarly to the resonant case. By perturbation calculation, we can show that the purity has
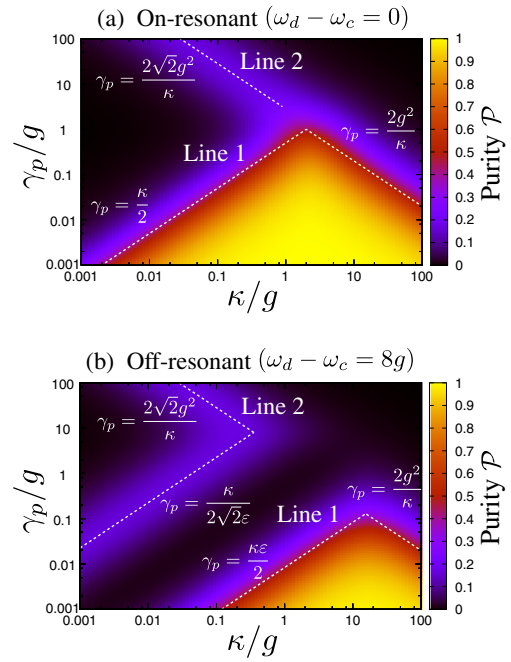

Fig. 9. (Color online) Purity calculated as a function of κ/g and $\gamma_{\rm p}/g$ for (a) the resonant case ($\omega_{\rm d} = \omega_{\rm c}$) and (b) the detuned case ($\omega_{\rm d} - \omega_{\rm c} = 8g$).

a maximum value of $\mathcal{P}_{\rm max} = 3 - 2\sqrt{2} \simeq 0.17$ at $\gamma_{\rm p} = \kappa/(2\sqrt{2}\varepsilon), 2\sqrt{2}g^2/\kappa$.

4.4 Time filtering

A strategy for improving the purity of emitted photons is to use photons emitted at the early stage of decay, because such photons are subject to the environment only for a short time. The density matrix of photons filtered in the temporal region $0 \leq t - r \leq T$ is written as $\rho_T(r, r', t) = \rho(r, r', t)\Theta(T - t + r)\Theta(T - t + r')$. From $\rho_T(r, r', t)$, the purity and efficiency of filtered photons are given as

$$\mathcal{P}(T) = \frac{{\rm Tr}(\rho_T^2)}{\mathcal{P}_{\rm d}(T)} = \frac{1}{\mathcal{P}_{\rm d}}\int_{t-T}^t {\rm d}r \int_{t-T}^t {\rm d}r' |\rho(r, r', t)|^2, \quad (50)$$

$$\mathcal{P}_{\rm d}(T) = [{\rm Tr}(\rho_T)]^2 = \left(\int_{t-T}^t {\rm d}r\, \rho(r, r, t)\right)^2, \quad (51)$$

where $\mathcal{P}_{\rm d}(T)$ is the square of the probability that a single photon is emitted during $0 \leq t \leq T$. $\mathcal{P}_{\rm d}(T)$ is also the square of the probability that a single photon is obtained after time filtering. By time filtering, the effective purity $\mathcal{P}(T)$ is improved at the expense of the square of the probability $\mathcal{P}_{\rm d}(T)$.

We first discuss the resonant ($\omega_{\rm d} = \omega_{\rm c}$) case. In Fig. 10(a), we show the T-dependence of $\mathcal{P}(T)$ and $\mathcal{P}_{\rm d}(T)$ for $\kappa/g = 2$ and $\gamma_{\rm p}/g = 0.5$. In the $T \to \infty$ limit, $\mathcal{P}(T)$ approaches 0.61, which is the purity without time filtering. As T is shortened, the purity $\mathcal{P}(T)$ increases, whereas the square of the probability $\mathcal{P}_{\rm d}(T)$ decreases. If we allow the reduction of the square of the probability to $1/2$, one can set the filtering time at $T = 2\tau_g$ [see the vertical dashed line in Fig. 10(a)], and obtain an improved purity of 0.85. Improvement of the purity is also possible in the detuned case. In Fig. 10(b), we show the T-dependence of $\mathcal{P}(T)$ and $\mathcal{P}_{\rm d}(T)$ for $\kappa/g = \sqrt{2}/50$, $\gamma_{\rm p}/g = 100$, and $\omega_{\rm d} - \omega_{\rm c} = 8g$, which is on the upper line of "Line 2" in Fig. 9(b). If we
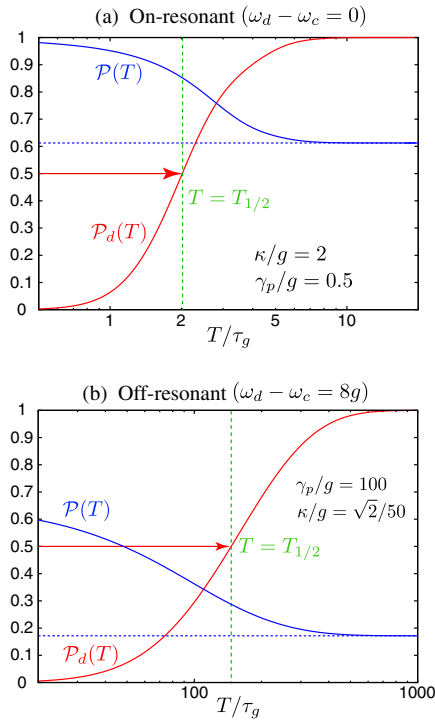
Fig. 10. (Color online) Effective purity $\mathcal{P}(T)$ and efficiency $\mathcal{P}_\mathrm{d}(T)$ of photons emitted to the output port during $0 < t < T$ shown as a function of T. (a) On-resonant case ($\omega_\mathrm{d} = \omega_c$) for $\kappa/g = 2$ and $\gamma_\mathrm{p}/g = 0.5$, and (b) detuned case ($\omega_\mathrm{d} - \omega_c = 8g$) for $\kappa/g = \sqrt{2}/50$ and $\gamma_\mathrm{p}/g = 100$. The time $T_{1/2}$ giving half-efficiency $\mathcal{P}_\mathrm{d}(T_{1/2}) = 1/2$ is also shown by a green line. The unit of time is given as $\tau_g = \hbar/g$ and is about 25 ps for $g = 25\,\mu\mathrm{eV}$.

allow the reduction of the square of the probability to 1/2, the purity is improved from 0.17 to 0.28.

We can improve the purity further by choosing a shorter filtering time. The efficiency, however, decreases exponentially in the limit $T \to 0$.

5. Summary

We analyzed the radiative decay of an excited dot in a solid-state cavity QED system and investigated the quantum–mechanical properties of the emitted photon, stressing the effects of pure dephasing. Our analysis is based on a model in which all the elements of the system (including environmental ones) are treated as active quantum–mechanical degrees of freedom. We rigorously solved the time evolution of the overall system and derived analytical

expressions for the density matrix, pulse shape, spectrum, and purity of the emitted photon. These analytical results were visualized under realistic parameters. The main results are summarized as follows. (i) Changes in the dot decay rate owing to pure dephasing can be explained in terms of the quantum Zeno and anti-Zeno effects. The emitted photon pulse length is approximately given by the inverse of the dot decay rate. (ii) The emitted photon spectrum agrees with the Glauber formula. The mean energy of an emitted photon is not necessarily identical to that of the dot and energy conservation is seemingly broken. However, the present analysis revealed that the dot can exchange energy with the environment through pure dephasing coupling. Energy conservation holds when the environmental energy is included. (iii) The purity of the emitted photon is calculated as a measure of indistinguishability. To generate pure single photons, dephasing should be reduced as much as possible and the escape rate of cavity photons κ should be taken near the optimal value ($\kappa = 2g$ for the resonant case and $\kappa = (2\sqrt{2}g^2/\epsilon)^{1/2}$ for the strongly detuned case). (iv) Time filtering improves the purity of the emitted photon at the expense of a lower probability of single photon generation.

In our approach, we have assumed white noise for the level fluctuation of the QD. For a detailed comparison with results of experiments, we must consider more realistic models taking into account phonons[35,36] and background carriers.[25] The extension of the present approach to these extended models is an important problem left for future study.

Appendix A: Relation to the Master Equation and Perturbation Method

To analyze the properties of emitted photons, one can employ the Master equation approach as an alternative method. The Master equation is derived for the present model as

$$
\frac{\mathrm{d}}{\mathrm{d}t}
\begin{pmatrix} \rho_{\sigma\sigma} \\ \rho_{\sigma a} \\ \rho_{a\sigma} \\ \rho_{aa} \end{pmatrix}
= -
\begin{pmatrix}
\gamma & ig & -ig & 0 \\
ig & \frac{\gamma+\kappa}{2} + \gamma_\mathrm{p} + i\Delta\omega & 0 & -ig \\
-ig & 0 & \frac{\gamma+\kappa}{2} + \gamma_\mathrm{p} - i\Delta\omega & ig \\
0 & -ig & ig & \kappa
\end{pmatrix}
\begin{pmatrix} \rho_{\sigma\sigma} \\ \rho_{\sigma a} \\ \rho_{a\sigma} \\ \rho_{aa} \end{pmatrix},
\tag{A$\cdot$1}
$$

where $\rho_{\sigma\sigma} = \langle \sigma^\dagger \sigma \rangle$, $\rho_{\sigma a} = \langle a^\dagger \sigma \rangle$, $\rho_{a\sigma} = \langle \sigma^\dagger a \rangle$, $\rho_{aa} = \langle a^\dagger a \rangle$, and $\Delta\omega = \omega_\mathrm{d} - \omega_\mathrm{c}$. Using the solution of the master equation, the density matrix $\rho(r, r', t)$ of emitted photons can be written as

$$
\rho(r, r', t) = \begin{cases}
\rho_{\sigma a}(t-r')\beta_0(r'-r) + \rho_{aa}(t-r')\tilde{\beta}_0(r'-r) & (r < r' < t), \\
\rho_{a\sigma}(t-r)\beta_0(r-r') + \rho_{aa}(t-r)\tilde{\beta}_0(r-r') & (r' < r < t).
\end{cases}
\tag{A$\cdot$2}
$$

Here, we have defined $(\tilde{\alpha}_0(t), \tilde{\beta}_0(t))$ as the solutions of Eq. (14) under the initial condition $(\tilde{\alpha}_0(0), \tilde{\beta}_0(0)) = (0, 1)$.

The four eigenvalues of the matrix in Eq. (A·1) correspond to the values of μ_i. Therefore, numerical calculation of the eigenvalues of this matrix is a convenient method for obtaining the values of μ_i. It is also useful to treat the matrix in Eq. (A·1) in the perturbation calculation given in Appendix B. Because the matrix in Eq. (A·1) is a normal matrix, it is diagonalized by a unitary matrix. Therefore, the perturbation method used in quantum mechanics can be applied to obtain the small shift of the values of μ_i with respect to small parameters.

Appendix B: Expressions for Purity in Limiting Cases

A simple expression for $\mathcal{P}$ can be obtained in some limiting cases. We first discuss the strongly detuned case ($|\omega_d - \omega_c| \gg g$). The purity can then be expressed by a sum of two contributions as $\mathcal{P} = \mathcal{P}_{\text{dot}} + \mathcal{P}_{\text{cav}}$, where $\mathcal{P}_{\text{dot}}$ and $\mathcal{P}_{\text{cav}}$ are the purities of photons whose frequencies are ω_d and ω_c, respectively.[37] The former contribution $\mathcal{P}_{\text{dot}}$ becomes large only below "Line 1" in Fig. 9(b), whereas $\mathcal{P}_{\text{cav}}$ has a maximum on "Line 2" in the figure. For $\gamma_p, \kappa \ll g$, perturbation calculation gives

$$\mathcal{P}_{\text{dot}} = \frac{\kappa}{2\gamma_p + \kappa} \times \frac{\kappa\varepsilon}{2\gamma_p + \kappa\varepsilon}. \quad (B\cdot1)$$

The first factor is the weight of the spectrum peak at $k = \omega_d$ [see Eq. (45)], and the second one is that due to spectrum broadening by pure dephasing. For large detuning ($\varepsilon \ll 1$), $\mathcal{P}_{\text{dot}}$ takes a value of $1/2$ around $\gamma_p = \varepsilon\kappa/2$, which corresponds to the left line of "Line 1" in Fig. 9(b). For $\gamma_p \ll g \ll \kappa$, perturbation calculation with respect to g is effective. Then, one can consider the effective continuum constructed by mixing between the cavity mode and the output mode (b field), and one can define the photon emission rate Γ from the dot into the effective continuum. By using Fermi's golden rule, the photoemission rate is estimated as $\Gamma = 2\pi g^2 D(\omega_d)$, where $D(\omega_d) = (\kappa/\pi)/[(\omega_d - \omega_c)^2 + (\kappa/2)^2]$ is the density of states of the effective continuum. In the presence of pure dephasing, the purity of photons emitted from a dot with the rate Γ is calculated as $\mathcal{P}_{\text{dot}} = 1/(1 + 2\gamma_p/\Gamma)$. Thus, we finally obtain

$$\mathcal{P}_{\text{dot}} = \frac{2g^2}{2g^2 + \gamma_p\kappa} \quad (B\cdot2)$$

for $\kappa \gg |\omega_d - \omega_c|$. One can see that the purity takes a value of $1/2$ at $\gamma_p = 2g^2/\kappa$, which corresponds to the right line of "Line 1" in Fig. 9(b). For $\gamma_p, \kappa \ll g$, perturbation calculation of $\mathcal{P}_{\text{can}}$ gives

$$\mathcal{P}_{\text{cav}} = \frac{2\gamma_p\varepsilon\kappa}{(\kappa + 2\gamma_p\varepsilon)(\kappa + 4\gamma_p\varepsilon)}. \quad (B\cdot3)$$

From this expression, it is proved that the purity takes a maximum value of $3 - 2\sqrt{2}$ at $\gamma_p = \kappa/(2\sqrt{2}\varepsilon)$, which corresponds to the lower line of "Line 2" in Fig. 9(b). For $\kappa \ll g \ll \gamma_p$, the dynamics of the cavity-dot system becomes completely incoherent and can be described by the rate equations

$$\dot{\rho}_{\sigma\sigma}(t) = -\Gamma'\rho_{\sigma\sigma}(t) + \Gamma'\rho_{aa}(t), \quad (B\cdot4)$$

$$\dot{\rho}_{aa}(t) = +\Gamma'\rho_{\sigma\sigma}(t) - \Gamma'\rho_{aa}(t) - \kappa\rho_{aa}(t), \quad (B\cdot5)$$

where $\rho_{\sigma\sigma}(t) = \langle\sigma^\dagger(t)\sigma(t)\rangle$, $\rho_{aa}(t) = \langle a^\dagger(t)a(t)\rangle$, and $\Gamma' = 2g^2/\gamma_p$ is the transition rate calculated from Fermi's golden rule. By solving these rate equations, we obtain

$$\mathcal{P}_{\text{cav}} = \frac{\kappa\Gamma'}{(\kappa + 2\Gamma')(\kappa + \Gamma')}. \quad (B\cdot6)$$

From this expression, it is proved that the purity takes a maximum value of $3 - 2\sqrt{2}$ at $\gamma_p = 2\sqrt{2}g^2/\kappa$, which corresponds to the upper line of "Line 2" in Fig. 9(b).

Next, we consider the resonant case ($\omega_c = \omega_d$). Some of the features are common to the strongly detuned case; the purity is reduced for $\kappa \geq 2g^2/\gamma_p$ [the right-side line of "Line 1" in Fig. 9(a)] and takes a maximum value of $3 - \sqrt{2}$ at $\gamma_p = 2\sqrt{2}g^2/\kappa$ ["Line 2" in Fig. 9(a)]. For $\gamma_p, \kappa \ll g$, the purity $\mathcal{P}$ is approximately calculated as

$$\mathcal{P} = \frac{\kappa(2\kappa + \gamma_p)}{2(\kappa + \gamma_p)(\kappa + 2\gamma_p)}. \quad (B\cdot7)$$

From this expression, it is proved that $\mathcal{P} \geq 1/2$ is realized for the condition $\kappa \geq (1 + \sqrt{3})\gamma_p \simeq 2.73\gamma_p$, which corresponds to the left line of "Line 1" in Fig. 9(a).

Appendix C: Relation between Coincidence Probability and Purity

Here, we derive the relation $P_{\text{co}} = (1 - \mathcal{P})/2$ between the coincidence probability P_{co} and the purity $\mathcal{P}$. We consider the following situation (see Fig. 4). Two solid-state emitters (S_1 and S_2) simultaneously and deterministically emit single photons (assuming $\gamma = 0$ for simplicity) into two input ports (P_1 and P_2) of a beam splitter. These two photons are mixed by the beam splitter and are output to ports P_3 and P_4. We denote the photon field operators for port P_j by $\tilde{b}_{(j)r}$ ($j = 1, \ldots, 4$), and the pure dephasing reservoir operators for emitter S_j by $\tilde{d}_{(j)r}$ ($j = 1, 2$). Assuming $t \to \infty$ and $\gamma = 0$ (and thus $\delta_m = 0$) in Eq. (13), the state vector of the photon at P_1 is given by

$$|\psi_1\rangle = \sum_{m=0}^{\infty} \int dr \, d^m x \, \gamma_m(t, r, x) \tilde{b}^\dagger_{(1)r} |x\rangle, \quad (C\cdot1)$$

where $|x\rangle = \tilde{d}^\dagger_{(1)x_1} \cdots \tilde{d}^\dagger_{(1)x_m} |0\rangle$. Thus, the emitted photon is entangled with the environment of its source. The input state vector including the photons at both P_1 and P_2 is then given by

$$|\psi_{12}\rangle = \sum_{m,n=0}^{\infty} \int dr \, dr' \, d^m x \, d^n x' \, \gamma_m(t, r, x) \gamma_n(t, r', x')$$
$$\times \tilde{b}^\dagger_{(1)r} \tilde{b}^\dagger_{(2)r'} |x; x'\rangle, \quad (C\cdot2)$$

where $|x; x'\rangle = \tilde{d}^\dagger_{(1)x_1} \cdots \tilde{d}^\dagger_{(1)x_m} \tilde{d}^\dagger_{(2)x'_1} \cdots \tilde{d}^\dagger_{(2)x'_n} |0\rangle$.

The beam splitter mixes the two photons as $\tilde{b}^\dagger_{(1)r} \to [\tilde{b}^\dagger_{(3)r} + \tilde{b}^\dagger_{(4)r}]/\sqrt{2}$ and $\tilde{b}^\dagger_{(2)r} \to [\tilde{b}^\dagger_{(3)r} - \tilde{b}^\dagger_{(4)r}]/\sqrt{2}$, but it obviously does not affect the environmental degrees of freedom. The output state vector is then given by $|\psi_{out}\rangle = |\psi_{33}\rangle + |\psi_{44}\rangle + |\psi_{34}\rangle$, where

$$|\psi_{33}\rangle = \sum_{m,n=0}^{\infty} \int dr \, dr' \, d^m x \, d^n x' \, \frac{\gamma_m(t, r, x) \gamma_n(t, r', x')}{2}$$
$$\times \tilde{b}^\dagger_{(3)r} \tilde{b}^\dagger_{(3)r'} |x; x'\rangle, \quad (C\cdot3)$$

$$|\psi_{44}\rangle = -\sum_{m,n=0}^{\infty} \int dr \, dr' \, d^m x \, d^n x' \, \frac{\gamma_m(t, r, x) \gamma_n(t, r', x')}{2}$$
$$\times \tilde{b}^\dagger_{(4)r} \tilde{b}^\dagger_{(4)r'} |x; x'\rangle, \quad (C\cdot4)$$

$$|\psi_{34}\rangle = \sum_{m,n=0}^{\infty} \int dr\,dr'\,d^m\boldsymbol{x}\,d^n\boldsymbol{x}'$$

$$\times\, \frac{\gamma_m(t,r,\boldsymbol{x})\gamma_n(t,r',\boldsymbol{x}') - \gamma_m(t,r',\boldsymbol{x})\gamma_n(t,r,\boldsymbol{x}')}{2}$$

$$\times\, \tilde{b}^{\dagger}_{(3)r}\tilde{b}^{\dagger}_{(4)r'}|\boldsymbol{x};\boldsymbol{x}'\rangle. \qquad (\text{C·5})$$

It is readily confirmed that $\langle\psi_{33}|\psi_{33}\rangle + \langle\psi_{44}|\psi_{44}\rangle + \langle\psi_{34}|\psi_{34}\rangle = 1$ and $\langle\psi_{33}|\psi_{33}\rangle = \langle\psi_{44}|\psi_{44}\rangle$. The coincidence probability P_{co} (i.e., the probability of finding single photons at both P_3 and P_4), is given by $P_{\text{co}} = \langle\psi_{34}|\psi_{34}\rangle$. Since the density matrix element is given by $\rho(r,r',t) = \sum_{m=0}^{\infty}\int d^m\boldsymbol{x}\,\gamma_m^*(r',\boldsymbol{x},t)\gamma_m(r,\boldsymbol{x},t)$, P_{co} is recast in the following form:

$$P_{11} = \frac{1}{2} - \frac{1}{2}\int dr\,dr'\,\rho(r,r',t)\rho(r',r,t) = \frac{1-\mathcal{P}}{2}. \qquad (\text{C·6})$$

When pure dephasing is present, the purity of the emitted photon will be less than unity and the coincidence probability will be nonzero.

Appendix D: Proof of Eqs. (48) and (49)

Here, we analytically evaluate $E_{\text{p}} = \int dk\,k\langle b_k^{\dagger}(t)b_k(t)\rangle_i$ and $E_{\text{e}} = \int dk\,k\langle d_k^{\dagger}(t)d_k(t)\rangle_i$ in the $t\to\infty$ limit, where $\langle\cdots\rangle_i = \langle\psi_i|\cdots|\psi_i\rangle$. Switching to real-space representations, we have

$$E_{\text{p}} = \frac{i}{2}\int dr\langle(\partial_r\tilde{b}^{\dagger}_r)\tilde{b}_r - \tilde{b}^{\dagger}_r(\partial_r\tilde{b}_r)\rangle_i, \qquad (\text{D·1})$$

$$E_{\text{e}} = \frac{i}{2}\int dr\langle(\partial_r\tilde{d}^{\dagger}_r)\tilde{d}_r - \tilde{d}^{\dagger}_r(\partial_r\tilde{d}_r)\rangle_i. \qquad (\text{D·2})$$

From Eq. (8), we obtain $\langle(\partial_r b_r^{\dagger})b_r\rangle_i = -\kappa\theta(t-\tau)\times\theta(\tau)\langle(\frac{d}{d\tau}a^{\dagger})a\rangle_i$, where $\tau = t - r$. Using similar equations, we have

$$E_{\text{p}} = -\frac{i\kappa}{2}\int_0^{\infty}d\tau\left\langle\left(\frac{d}{d\tau}a^{\dagger}\right)a - a^{\dagger}\left(\frac{d}{d\tau}a\right)\right\rangle_i, \qquad (\text{D·3})$$

$$E_{\text{e}} = -i\gamma_{\text{p}}\int_0^{\infty}d\tau\left\langle\left(\frac{d}{d\tau}\sigma^{\dagger}\sigma\right)\sigma^{\dagger}\sigma - \sigma^{\dagger}\sigma\left(\frac{d}{d\tau}\sigma^{\dagger}\sigma\right)\right\rangle_i. \qquad (\text{D·4})$$

Using Eqs. (11) and (12) and their conjugates, we have

$$E_{\text{p}} = \kappa\omega_{\text{c}}\int_0^{\infty}d\tau\langle a^{\dagger}a\rangle + \frac{g\kappa}{2}\int_0^{\infty}d\tau(\langle a^{\dagger}\sigma\rangle + \langle\sigma^{\dagger}a\rangle), \qquad (\text{D·5})$$

$$E_{\text{e}} = g\gamma_{\text{p}}\int_0^{\infty}d\tau(\langle a^{\dagger}\sigma\rangle + \langle\sigma^{\dagger}a\rangle). \qquad (\text{D·6})$$

Thus, we must evaluate $I_1 = \int_0^{\infty}d\tau\langle\sigma^{\dagger}\sigma\rangle$, $I_2 = \int_0^{\infty}d\tau\langle a^{\dagger}a\rangle$, and $I_3 = \int_0^{\infty}d\tau\langle\sigma^{\dagger}a\rangle$.

The equations of motion for $\langle\sigma^{\dagger}\sigma\rangle$, $\langle a^{\dagger}a\rangle$, and $\langle\sigma^{\dagger}a\rangle$ are given by

$$\frac{d}{dt}\langle\sigma^{\dagger}\sigma\rangle = -\gamma\langle\sigma^{\dagger}\sigma\rangle - ig(\langle\sigma^{\dagger}a\rangle - \text{c.c.}), \qquad (\text{D·7})$$

$$\frac{d}{dt}\langle a^{\dagger}a\rangle = -\kappa\langle a^{\dagger}a\rangle + ig(\langle\sigma^{\dagger}a\rangle - \text{c.c.}), \qquad (\text{D·8})$$

$$\frac{d}{dt}\langle\sigma^{\dagger}a\rangle = i(\tilde{\omega}_{\text{d}}^* - \tilde{\omega}_{\text{c}})\langle\sigma^{\dagger}a\rangle + ig(\langle a^{\dagger}a\rangle - \langle\sigma^{\dagger}\sigma\rangle). \qquad (\text{D·9})$$

Integrating these equations with respect to τ, we obtain $1 = \gamma I_1 + ig(I_3 - I_3^*)$, $\quad 0 = \kappa I_2 - ig(I_3 - I_3^*)$, $\quad 0 = i(\tilde{\omega}_{\text{d}}^* - \tilde{\omega}_{\text{c}})I_3 + ig(I_2 - I_1)$. When $\gamma = 0$, these equations are solved to yield $I_2 = 1/\kappa$ and $I_3 = (i/g)\times(\tilde{\omega}_{\text{c}}^* - \tilde{\omega}_{\text{d}})/(\tilde{\omega}_{\text{c}} + \tilde{\omega}_{\text{d}} - \tilde{\omega}_{\text{c}}^* - \tilde{\omega}_{\text{d}}^*)$. Since $E_{\text{p}} = \kappa\omega_{\text{c}}I_2 + (g\kappa/2)(I_3 + I_3^*)$ and $E_{\text{e}} = g\gamma_{\text{p}}(I_3 + I_3^*)$, we obtain Eqs. (48) and (49).

*kazuki.koshino@osamember.org

1) R. Miller, T. E. Northup, K. M. Birnbaum, A. Boca, A. D. Boozer, and H. J. Kimble: J. Phys. B **38** (2005) S551.
2) G. Khitrova, H. M. Gibbs, M. Kira, S. W. Koch, and A. Scherer: Nat. Phys. **2** (2006) 81.
3) J. P. Reithmaier, G. Sęk, A. Löffler, C. Hofmann, S. Kuhn, S. Reizenstein, L. V. Keldysh, V. D. Kulakovskii, T. L. Reinecke, and A. Forchel: Nature **432** (2004) 197.
4) T. Yoshie, A. Scherer, J. Hendrickson, G. Khitova, H. M. Gibbs, G. Rupper, C. Ell, O. B. Shchekin, and D. G. Deppe: Nature **432** (2004) 200.
5) E. Peter, P. Senellart, D. Martrou, A. Lemaître, J. Hours, J. M. Gérard, and J. Bloch: Phys. Rev. Lett. **95** (2005) 067401.
6) S. Strauf, K. Hennessy, M. T. Rakher, Y.-S. Choi, A. Badolato, L. C. Andreani, E. L. Hu, P. M. Petroff, and D. Bouwmeester: Phys. Rev. Lett. **96** (2006) 127404.
7) K. Srinivasan and O. Painter: Nature **450** (2007) 862.
8) K. Srinivasan and O. Painter: Phys. Rev. A **75** (2007) 023814.
9) P. Michler, A. Kiraz, C. Becher, W. V. Schoenfeld, P. M. Petroff, L. Zhang, E. Hu, and A. Imamoğlu: Science **290** (2000) 2282.
10) C. Santori, M. Pelton, G. Solomon, Y. Dale, and Y. Yamamoto: Phys. Rev. Lett. **86** (2001) 1502.
11) E. Moreau, I. Robert, J. M. Gérard, I. Abram, L. Manin, and V. Thierry-Mieg: Appl. Phys. Lett. **79** (2001) 2865.
12) C. Santori, D. Fattal, J. Vuckovic, G. S. Solomon, and Y. Yamamoto: Nature **419** (2002) 594.
13) S. Varoutsis, S. Laurent, P. Kramper, A. Lemaître, I. Sagnes, I. Robert-Philip, and I. Abram: Phys. Rev. B **72** (2005) 041303.
14) D. Fattal, K. Inoue, J. Vučković, C. Santori, G. S. Solomon, and Y. Yamamoto: Phys. Rev. Lett. **92** (2004) 037903.
15) A. Kiraz, M. Atatüre, and A. Imamoğlu: Phys. Rev. A **69** (2004) 032305.
16) K. Hennessy, A. Badolato, M. Wigner, D. Gerace, M. Atatüre, S. Gulde, S. Fält, E. L. Hu, and A. Imamoğlu: Nature **445** (2007) 896.
17) A. Muller, E. B. Flagg, P. Bianucci, X. Y. Wang, D. G. Deppe, W. Ma, J. Zhang, G. J. Salamo, M. Xiao, and C. K. Shih: Phys. Rev. Lett. **99** (2007) 187402.
18) D. Press, S. Gotzinger, S. Reitzenstein, C. Hofmann, A. Loffler, M. Kamp, A. Forchel, and Y. Yamamoto: Phys. Rev. Lett. **98** (2007) 117402.
19) J. Suffczyński, A. Dousse, K. Gauthron, A. Lemaitre, I. Sagnes, L. Lanco, J. Bloch, P. Voisin, and P. Senellart: Phys. Rev. Lett. **103** (2009) 027401.
20) Y. Ota, N. Kumagai, S. Ohkouchi, M. Shirane, M. Nomura, S. Ishida, S. Iwamoto, S. Yorozu, and Y. Arakawa: Appl. Phys. Express **2** (2009) 122301.
21) S. Ates, S. M. Ulrich, A. Ulhaq, S. Reitzenstein, A. Löffler, S. Höfling, A. Forchel, and P. Michler: Nat. Photonics **3** (2009) 724.
22) A. Ulhaq, S. Ates, S. Weiler, S. M. Ulrich, S. Reitzenstein, A. Löffler, S. Höfling, L. Worschech, A. Forchel, and P. Michler: Phys. Rev. B **82** (2010) 045307.
23) G. Cui and M. G. Raymer: Phys. Rev. A **73** (2006) 053807 [Erratum **78** (2008) 049904].
24) A. Naesby, T. Suhr, P. T. Kristensen, and J. Mork: Phys. Rev. A **78** (2008) 045802.
25) M. Yamaguchi, T. Asano, and S. Noda: Opt. Express **16** (2008) 18067.
26) A. Auffèves, J.-M. Gérard, and J.-P. Poizat: Phys. Rev. A **79** (2009) 053838.
27) A. Auffèves, D. Gerace, J.-M. Gérard, M. F. Santos, L. C. Andreani, and J.-P. Poizat: Phys. Rev. B **81** (2010) 245419.
28) K. Koshino and A. Shimizu: Phys. Rep. **412** (2005) 191.
29) K. Koshino: Phys. Rev. A **84** (2011) 033824.
30) D. Walls and G. J. Milburn: Quantum Optics (Springer, New York, 1995).
31) C. W. Gardiner and P. Zoller: Quantum Noise (Springer, New York, 2004).
32) R. J. Glauber: in Quantum Optics and Electronics, ed. C. de Witt, A. Blandin, and C. Cohen-Tannoudji (Gordon and Breach, New York, 1965) p. 65.
33) A. G. Kofman and G. Kurizki: Phys. Rev. Lett. **87** (2001) 270405.
34) A. Shnirman and Yu. Makhlin: JETP Lett. **78** (2003) 447.
35) G. Tarel and V. Sanova: Phys. Rev. B **81** (2010) 075305.
36) P. Kaer, T. R. Nielsen, P. Lodahl, A.-P. Jauho, and J. Mørk: Phys. Rev. Lett. **104** (2010) 157401.
37) By using a frequency filtering technique, we can extract one of the two contributions to the purity. However, frequency filtering is shown to be ineffective for improving the purity.